



Observed decreases in on-road CO₂ concentrations in Beijing during COVID-19 restrictions

Di Liu¹, Wanqi Sun², Ning Zeng^{3,4}, Pengfei Han¹, Bo Yao², Zhiqiang Liu¹, Pucai Wang⁵, Ke Zheng¹, Han Mei¹, and Qixiang Cai¹

¹Laboratory of Numerical Modeling for Atmospheric Sciences & Geophysical Fluid Dynamics, Institute of Atmospheric Physics, Chinese Academy of Science, Beijing, China

²Meteorological Observation Centre, China Meteorological Administration, Beijing, China

³Department of Atmospheric and Oceanic Science, University of Maryland, College Park, MD, USA

⁴Earth System Science Interdisciplinary Center, University of Maryland, College Park, MD, USA

⁵Laboratory for Middle Atmosphere and Global Environment Observation, Institute of Atmospheric Physics, Chinese Academy of Sciences, Beijing, China

Correspondence: Pengfei Han (pphan@mail.iap.ac.cn) and Bo Yao (yaob@cma.gov.cn)

Received: 16 September 2020 – Discussion started: 12 October 2020

Revised: 3 February 2021 – Accepted: 13 February 2021 – Published: 25 March 2021

Abstract. To prevent the spread of the COVID-19 epidemic, restrictions such as “lockdowns” were conducted globally, which led to a significant reduction in fossil fuel emissions, especially in urban areas. However, CO₂ concentrations in urban areas are affected by many factors, such as weather, biological sinks and background CO₂ fluctuations. Thus, it is difficult to directly observe the CO₂ reductions from sparse ground observations. Here, we focus on urban ground transportation emissions, which were dramatically affected by the restrictions, to determine the reduction signals. We conducted six series of on-road CO₂ observations in Beijing using mobile platforms before (BC), during (DC) and after (AC) the implementation of COVID-19 restrictions. To reduce the impacts of weather conditions and background fluctuations, we analyze vehicle trips with the most similar weather conditions possible and calculated the enhancement metric, which is the difference between the on-road CO₂ concentration and the “urban background” CO₂ concentration measured at the tower of the Institute of Atmospheric Physics (IAP), Chinese Academy of Sciences. The results showed that the DC CO₂ enhancement was decreased by 41 (±1.3) parts per million (ppm) and 26 (±6.2) ppm compared to those for the BC and AC trips, respectively. Detailed analysis showed that, during COVID-19 restrictions, there was no difference between weekdays and weekends during working hours (09:00–17:00 local standard time;

LST). The enhancements during rush hours (07:00–09:00 and 17:00–20:00 LST) were almost twice those during working hours, indicating that emissions during rush hours were much higher. For DC and BC, the enhancement reductions during rush hours were much larger than those during working hours. Our findings showed a clear CO₂ concentration decrease during COVID-19 restrictions, which is consistent with the CO₂ emissions reductions due to the pandemic. The enhancement method used in this study is an effective method to reduce the impacts of weather and background fluctuations. Low-cost sensors, which are inexpensive and convenient, could play an important role in further on-road and other urban observations.

1 Introduction

Since December 2019, the world has been fiercely struggling with a pandemic of a novel coronavirus named COVID-19, which was first identified in Wuhan, China (Gross et al., 2020), and then quickly identified in other countries of East Asia, Europe and the United States according to World Health Organization Novel Coronavirus (2019-nCoV) situation reports (<https://www.who.int/emergencies/diseases/novel-coronavirus-2019/situation-reports>, last access: December 2020). In Beijing, the first case was confirmed on

20 January 2020, followed by a quick increase in confirmed cases (Fig. S1A). From 24 January to 30 April, Beijing enacted a level-1 response to major public health emergencies (red region in Fig. S1) and lowered the response to level 2 from 30 April to 6 June, after “zero growth” persisted for almost 1 month (yellow region in Fig S1).

As the world faced this highly infectious pandemic without efficient medication, governments enacted similar restrictions to prevent the spread of the virus: isolating cases, enacting stay-at-home orders, forbidding mass gatherings and closing factories and schools. These restrictions highly altered the industrial production, energy consumption and transportation volume and led to sharp emission reductions (Liu et al., 2020; Le Quere et al., 2020). As previous inventory studies estimated, by early April 2020, the global daily CO₂ emissions had decreased by 17 % (11 % to 25 % for $\pm 1\sigma$) compared with those in 2019, and the total reduction was approximately 1048 (543 to 1638) MtCO₂ at the end of April (Le Quere et al., 2020). Emissions from ground transportation obviously decreased by 36 % (Le Quere et al., 2020). According to Liu et al. (2020), emissions in China decreased 7 % from January to April 2020, with ground transportation emissions dropping abruptly by 53 % in February and continuing to decrease by 26 % in March (Fig. S1B and S1C). In Beijing, during the first quarter of 2020, passenger traffic volumes decreased 56 %, and ground transport volumes decreased 35 % according to the distance-weighted passenger and freight turnover (Han et al., 2020).

Urban areas are the main CO₂ sources and account for more than 70 % of fossil fuel emissions (Rosenzweig et al., 2010), and CO₂ concentrations in urban areas are dominated by weather changes (Woodwell et al., 1973; Grimmond et al., 2002); for example, high wind speed accelerates the mixing and diffusion of CO₂. In addition, the carbon emission reductions (258 MtC, from Le Quere et al., 2020) due to COVID-19 restrictions were relatively small compared to the CO₂ content in the atmosphere (860 GtC, from Friedlingstein et al., 2019) and carbon uptake by vegetation (the average seasonal amplitude of the net land–atmosphere carbon flux is 41.6 GtC yr^{−1}, from Zeng et al. (2014)). Therefore, it is difficult to detect CO₂ concentration decreases in the urban areas directly from sparse ground observations (Kutsch et al., 2020; Ott et al., 2020). For example, according to the daily CO₂ concentrations in 2019 and 2020 recorded by the tower at the Institute of Atmospheric Physics (IAP), Chinese Academy of Sciences, even though Beijing was within the strictest control/confinement period from 10 to 14 February 2020, stable weather (in which the planetary boundary layer heights (PBLHs) were only ~ 600 m) led to CO₂ concentrations that were approximately 90 ppm higher than those on the same date in 2019 (PBLHs were ~ 900 m) (Fig. 1D). Sussmann and Rettinger (2020) also proved it. Despite global emission reductions due to COVID-19 restrictions, they found a historic record high in column-averaged atmospheric carbon dioxide (XCO₂) in April 2020 by us-

ing Total Carbon Column Observation Network (TCCON) data. By assuming that the COVID-19-related CO₂ growth rate reduction of 0.32 ppm yr^{−2} in 2020 at Mauna Loa is true and measured (from the UK Met Office; an overall 8 % emission reduction in 2020), they found that there is a ~ 0.6 year “delay” to separate TCCON-measured growth rates and the reference forecast (absence of COVID-19 restrictions).

With the knowledge that urban ground transportation was strongly suppressed due to COVID-19 restrictions, we designed on-road observations by using a mobile platform to detect reduction signals. These observations could provide CO₂ data with higher spatiotemporal resolution than satellite and ground observations and have been widely used for carbon monitoring in urban and suburban areas (for instance, on-road CO₂ concentration distributions were presented as transects in urban areas along routes) (Idso et al., 2001; Bush et al., 2015; Sun et al., 2019). Almost all studies agreed that weather (for example, wind speed, which is directly associated with CO₂ mixing and dilution) is a dominant factor and should be considered during analysis. Reducing the impact of weather is still problematic. On the other hand, examining the enhancement, which is the calculated difference in the CO₂ concentration between urban and rural background observations, could effectively reduce the influence of background CO₂ fluctuations, and this metric has been widely used for monitoring urban carbon emissions and CO₂ concentrations (Idso et al., 1998, 2002; George et al., 2007; Mitchell et al., 2018; Perez et al., 2009).

To determine the CO₂ concentration reduction “signal” due to decreased ground transportation emissions during COVID-19 restrictions, we chose the most similar weather conditions possible and calculated the enhancements metric by subtracting the “baseline” IAP tower CO₂ concentration from the observed on-road CO₂ concentration to reduce impact of background CO₂ fluctuations. Our results may provide direct evidence of ground transportation emission reductions due to COVID-19 restrictions, and this method could be an appropriate tool to analyze the CO₂ concentration and emissions related to urban ground transportation in future works.

2 Methods and data

We conducted six on-road observations in Beijing using mobile platforms before (BC; one trip: 20 February 2019), during (DC; four trips: 13, 20, 21 and 22 February 2020) and after (AC; one trip: 9 May 2020) COVID-19 restrictions (vertical lines in Fig. S1 indicate the trip dates). These trips covered four ring roads that circled the city: the second (with length of 33 km), third (48 km), fourth (64 km) and fifth (99 km) ring roads, from innermost to outermost, as shown in Fig. 1. All trips were conducted during the daytime; four of them were on weekdays and two others were on a Saturday. Four trips covered at least one rush hour (07:00–09:00

local standard time (LST) for the morning rush hour; 17:00–20:00 LST for the evening).

To reduce the influence of background CO₂ fluctuations, we chose similar weather conditions. As shown in Table 1, four aspects were considered: (1) real-time panoramic photographs collected from the IAP tower (photograph available from <http://view.iap.ac.cn:8080/imageview/>, last access: May 2020); (2) the PM_{2.5} (atmospheric particulate matter with a diameter of less than 2.5 µm) concentration from the Olympic Sports Center Station (40.003° N, 116.407° E; 5 m height, purple square in Fig. 1a), which is run by the Ministry of Ecology and Environment of China (Zhang et al., 2015); (3) wind speed data (collected from <https://www.wunderground.com/history/daily/cn/beijing/ZBNY/date/2020-5-9>, last access: May 2020); and (4) PBLH data, which are related to vertical mixing and diffusion of pollution and/or CO₂ emitted near the ground (Su et al., 2018). These data were collected from National Centers for Environmental Prediction Global Forecast System (GFS) reanalysis dataset (resolution: 0.25° × 0.25°), which is a globally gridded dataset representing the state of the Earth's atmosphere and incorporating observations and numerical weather prediction model output.

Then, on-road CO₂ concentration enhancements were calculated by subtracting the simultaneous CO₂ concentrations detected at the IAP tower, which served as the “baseline” for the city of Beijing (Eq. 1).

$$\text{CO}_2\text{enhancement} = \text{CO}_2(\text{on-road}) - \text{CO}_2(\text{IAP tower}) \quad (1)$$

3 CO₂ concentration at the IAP tower

The IAP tower is a 325 m high meteorological tower located at 39.9667° N, 116.3667° E, 49 m above sea level in north-west Beijing (Fig. 1, black triangle) (Cheng et al., 2018). The CO₂ concentration was determined at three levels in this study: surface level (~ 2 m above the ground), lower level (~ 80 m) and upper level (~ 280 m). The CO₂ concentrations were measured by a Picarro G2301 greenhouse gas concentration analyzer (Picarro, 2019). The instrument was calibrated by using standard gas for every 3 h, and each calibration lasted 5 min. The standard gases were from the Meteorological Observation Center of the China Meteorological Administration (MOC/CMA) and were traced to the World Meteorological Organization (WMO) X2007 scale. The measurement accuracy was ~ 0.1 ppm. The CO₂ concentration was recorded by every 2 s, and these data were averaged into 1 min intervals. Before 2020 (including the trip on 20 February 2019), the CO₂ concentration was measured at the lower and upper levels alternately for every 5 min, and the measurement at each level lasted 5 min. After 2020 (including the other five trips), the CO₂ concentration was continuously measured at the surface level. To maintain consistency as much as possible, we used the lower-level CO₂ before 2020 and the surface-level CO₂ after 2020.

4 On-road CO₂ concentration data

Three different CO₂-observing instruments were carried by vehicles during six on-road trips (Table 2).

1. On 20 February 2019, a Picarro G2401 (Picarro, 2017) was installed on a vehicle; the air intake was set on the roof of the vehicle to avoid contact with direct plumes emitted from surrounding cars. The intake was linked/connected through a 2 m pipe with a particulate matter filter to the Picarro system (Fig. 2a and b). The instrument characteristics and accuracy have been described by Sun et al. (2019). The CO₂ concentrations were collected every 2 s and then averaged into 1 min intervals.
2. During COVID-19 restrictions (surveys on 13, 20, 21 and 22 February 2020), a LI-COR LI-7810 CH₄/CO₂/H₂O trace gas analyzer was adopted, which uses optical feedback cavity-enhanced absorption spectroscopy (LI-COR, 2019). This instrument could obtain a CO₂ concentration with a precision of 3.5 ppm for 1 s and within 1 ppm after 1 min averaging (laboratory testing). The observation platform of the LI-7810 was similar to that of the Picarro system. Before departure, the instrument was calibrated by using standard calibration gas to correct the drift.
3. On 9 May 2020, a low-cost light sensor was adopted and installed on the front windshield of the vehicle (Fig. 2c). The instrument mainly consisted of three non-dispersive infrared (NDIR) CO₂ measurement sensors (named K30) and one environment (temperature, humidity and pressure) sensor (named BME). Although the original precision of each K30 was ±30 ppm, after calibration and environmental correction in the laboratory and before departure, the accuracy was improved to within ±5 ppm in comparison to Picarro (Martin et al., 2017; SenseAir, 2019). Here, we used three K30s in one instrument to recognize and eliminate data anomalies and used the average CO₂ concentrations from the three K30s for analysis. Figure 3 shows the details of the experiment conducted on 22 February 2020, for which one low-cost light sensor and Picarro were installed on the same vehicle for on-road monitoring. The results showed that the low-cost light sensor results were highly consistent with those of the Picarro system, with root mean square errors (RMSEs) less than 5 ppm.

5 Auxiliary data and analysis

The Global Positioning System (GPS) data for BC and DC were collected by a GPS receiver (BS-70DU) (Sun et al., 2019). For AC, the data were collected by using mobile software (GPS Tracks), which provided time, longitude, latitude,

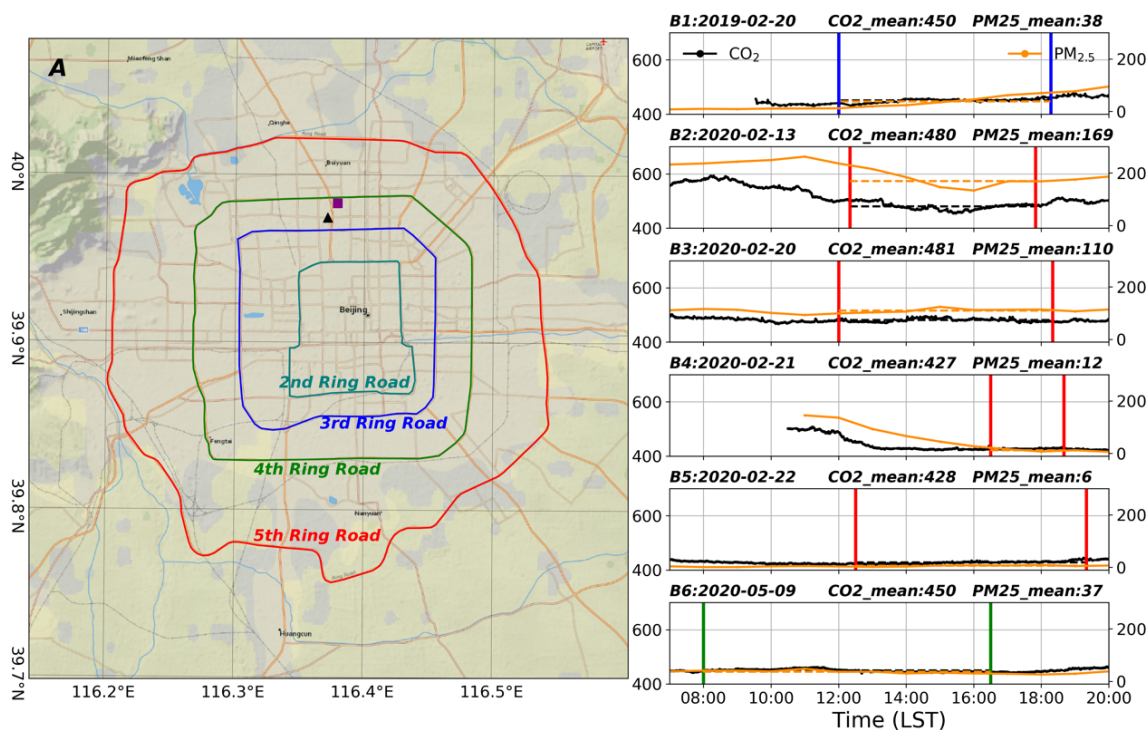


Figure 1. A: the locations of the second, third, fourth and fifth ring roads, the IAP tower (black triangle) and Olympic Sports Center station (purple square); B1–B6: CO₂ concentration at the IAP tower and PM_{2.5} concentration data from the Olympic Sports Center station during six trips.

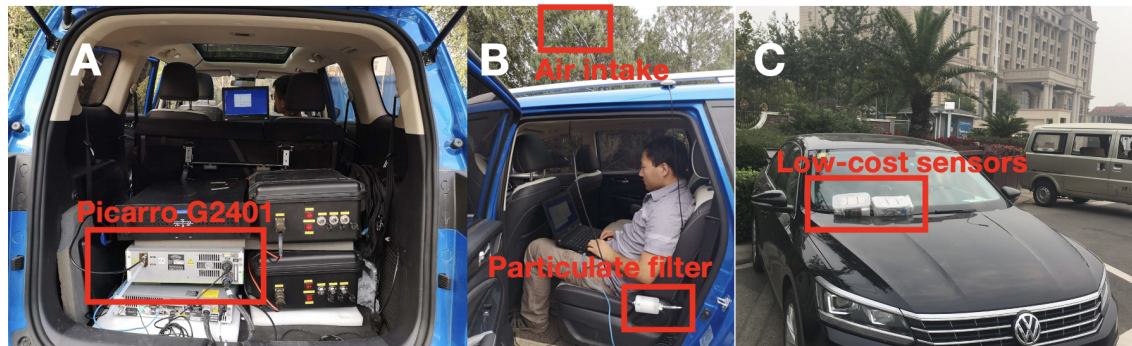


Figure 2. Photographs of the instrument installation for the on-road observations. (a–b) Picarro system installed in the vehicle; (c) low-cost non-dispersive infrared (NDIR) sensors installed on the front windshield of the vehicle.

speed and altitude at 1 s resolution. These geographic information data were averaged into 1 min intervals and then matched with the CO₂ concentration data according to time.

Two remote sensing images were adopted (captured on 21 February 2019 at 11:40:00 LST from a Google Earth image, with 0.37 m spatial resolution; 19 February 2020 at 10:20:08 LST from a Beijing-2 remote sensing satellite panchromatic image, with 0.8 m spatial resolution). Considering the availability of data, we used the images from the closest date and only part of the urban area. The comparison region covered 10 km of the third ring road (accounting for 21 % of the whole road) and 13.4 km of the fourth ring road

(also 21 % of the whole road). We used a visual interpretation method to obtain the numbers of vehicles on the third and fourth ring roads for BC and DC, respectively.

To understand the traffic situation, we also collected the real-time traffic congestion conditions (for each road), road name, geographic information, road type and average speed as 1 h data from the AutoNavi open platform (<https://lbs.amap.com/>, last access: May 2020).

Table 1. Weather conditions during six trips.

Label/date yyyy-mm-dd	Weather condition	Air condition (PM _{2.5} : µg m ⁻³)	Wind speed (m s ⁻¹)	PBLH (m)	Real-time panoramic photographs
BC 2019-2-20 (Wed)	Clear day	38	2.5	897.7	
DC 2020-2-13 (Fri)	Heavily polluted day	169	2.5	589	
DC 2020-2-20 (Fri)	Lightly polluted day	110	1.3	691	
DC 2020-2-21 (Fri)	Clear day	12	2.5	1587	
DC 2020-2-22 (Fri)	Clear day	6	3.6	1113	

Table 1. Continued.


Label/date yyyy-mm-dd	Weather condition	Air condition (PM _{2.5} : µg/m ³)	Wind speed (m s ⁻¹)	PBLH (m)	Real-time panoramic photographs
AC 2020-5-9 (Sat)	Clear day	37	1.6	608	

Table 2. Instrument parameters for six on-road observations.

Label	Date	Instrument	Accuracy	Temporal resolution (original → processed)
BC	2019-2-20	Picarro G2401	±0.1 ppm	2 s → 1 min
DC				
	2020-2-13	LI-COR LI-7810	±3.5 ppm (for 1 s);	
	2020-2-20	LI-COR LI-7810	improved into ±1 ppm	1 s → 1 min
	2020-2-21	LI-COR LI-7810	(for 1 min)	
	2020-2-22	LI-COR LI-7810		
AC	2020-5-9	Low-cost Sensor (K30)	±5 ppm	2 s → 1 min

6 Results

6.1 On-road CO₂ concentration

The CO₂ concentration maps of six on-road trips are shown in Fig. 4. According to Table 1, we selected four trips as the trips with the most similar weather conditions: one BC trip (20 February 2019; Fig. 4a), two DC trips (21 and 22 February 2020; Fig. 4d and e) and one AC trip (9 May 2020; Fig. 4f). Statistically, the average of the two DC trips was 444 (±1) ppm, which was 69 (±1.1) and 57 (±6) ppm lower than that of the BC and AC trips, respectively. The other two DC trips (13 and 20 February) were conducted on (lightly/heavily) polluted days, and the CO₂ concentrations on these two days were as high as those during the BC and AC trips.

We chose one DC trip (21 February 2020) for further analysis and compared it to the BC and AC trips. All three trips were conducted on clear days, and their trajectories were similar, from the outermost circle to the innermost circle, and covered one (morning or evening) rush hour. The difference was that the BC and DC trips hit the evening rush hour on the innermost ring road, whereas the AC trip hit the morning rush hour on the outermost ring road. This difference explained

why the CO₂ concentration was high on the innermost road (second ring road) in Fig. 4a and d and on the outermost road (fifth ring road) in Fig. 4f. The comparison of the three trips indicated that the CO₂ concentration in Fig. 4d was lower than those in Fig. 4a and f, and the statistics show that the mean CO₂ of the DC trips was approximately 58 (±1.1) and 46 (±6) ppm lower than those of the BC and AC trips, respectively. In addition, the average CO₂ concentration observed at the IAP tower during the same periods was much lower than the on-road observations (Fig. 1B). These concentration differences (gradients) also implied that ground transportation emissions were a major CO₂ source on these urban roads.

However, it was difficult to completely eliminate the impact of background CO₂ fluctuations only through selecting trips with the most similar weather conditions. For example, the PBLHs during two DC trips with the most similar weather were 1587 and 1113 m, which were almost twice of those during the BC and AC trips (Table 1). The CO₂ concentrations at the IAP tower also indicated that during these two DC trips, the CO₂ concentrations were 427 (±0.1) and 428 (±0.1) ppm, which were approximately 20 ppm lower than those for the BC and AC trips (in Fig. 1).

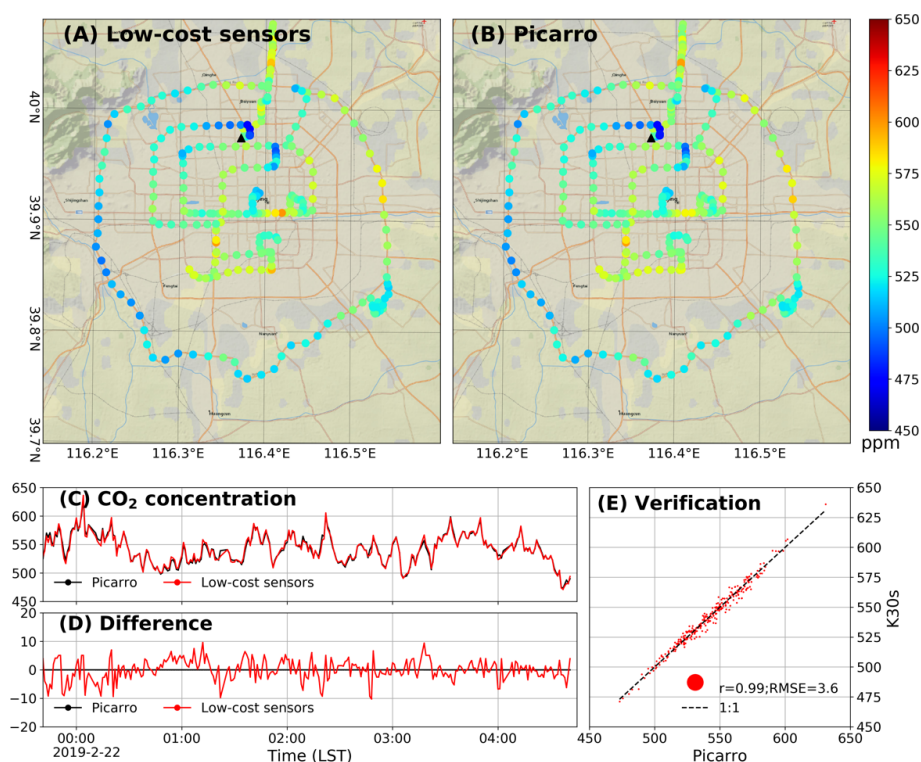


Figure 3. Verification of low-cost sensors for on-road observations. (a) Map of CO₂ concentrations measured by the low-cost sensor; (b) map of the CO₂ concentration measured by the Picarro system on the same vehicle; (c) time series of the CO₂ concentrations measured by the low-cost sensor and Picarro system; (d) difference (low-cost sensor concentration minus Picarro concentration); (e) scatter plot of the low-cost sensor and Picarro data, with an RMSE of 3.6 ppm.

6.2 On-road CO₂ enhancement

To further reduce the influence of background CO₂ variations, we calculated the CO₂ enhancement for six trips by subtracting the CO₂ concentration at IAP tower from the on-road CO₂ concentration (shown in Fig. 5). The spatial distribution patterns of the enhancement were similar to the distribution of the CO₂ concentration maps, in which the enhancements during rush hours were much higher for all trips. Furthermore, the refined spatial distribution of the CO₂ gradient implied emissions from ground transportation.

It is worth noting that the enhancements for the four DC trips were almost the same, although the weather conditions (based on the PBLH, PM_{2.5} and wind speed data) during these trips were quite different. However, the DC enhancements were obviously different from the BC and AC enhancements. During the two DC trips on polluted days (13 and 20 February 2020), the mean CO₂ concentrations were similar to those during the BC and AC trips (Fig. 4b and c); however, the enhancements extracted the traffic emission signals from the background, with averages of 33 (± 1.1) and 16 (± 1.1) ppm (Fig. 5b and c). Statistically, the average of the four DC enhancements was 24 (± 1.1) ppm, which was 41 (± 0.2) and 26 (± 6.2) ppm lower than those of the BC and AC enhancements.

6.3 Diurnal variation analysis

Figure 6 shows the diurnal variation in the CO₂ concentrations from IAP tower observations, on-road CO₂ concentrations, enhancements and trajectories. In Fig. 6a, the CO₂ concentrations measured at the IAP tower were stable and showed an approximate 50 ppm difference between trips. The CO₂ concentrations at the IAP tower during the first two DC trips (13 and 20 February 2020) were ~ 30 ppm higher than those during the BC and AC trips. However, the CO₂ concentrations during the other two DC trips (21 and 22 February 2020) were ~ 20 ppm lower than those during the BC and AC trips. These “baseline” CO₂ concentration fluctuations make the on-road observations not directly comparable. In Fig. 7b, the CO₂ concentrations show a “double-peak” pattern, with peaks during the morning (07:00–09:00 LST) and evening (17:00–20:00 LST) rush hours. During the rush hours, the CO₂ concentrations ranged from 500 to 600 ppm, which were approximately 100 ppm higher than the concentrations during working hours (09:00–17:00 LST). The comparison of BC and AC indicates that the CO₂ concentrations measured on 13 and 20 February 2020 did not significantly decrease during 12:00–17:00 LST. However, the CO₂ concentrations measured on 21 and 22 February 2020 were much lower (~ 50 ppm) than those measured

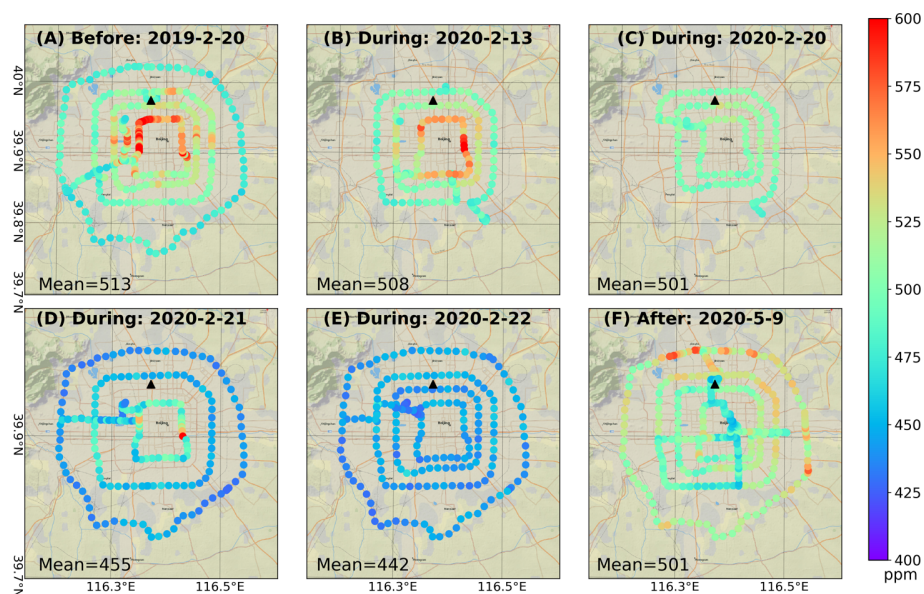


Figure 4. CO₂ concentration maps for six on-road trips. Circles mark the locations of CO₂ concentration records taken at a 1 min interval (see methods). All subplots have the same color scale, ranging from 400 to 600 ppm. The black triangle is the location of the IAP tower. One trip (a: 20 February 2019) was conducted before the COVID-19 restrictions, with an average of 513 (with an instrument uncertainty of ± 0.1) ppm. Four trips (b–e: 13, 20, 21 and 22 February 2020) were conducted during COVID-19 restrictions, with averages of 508 (± 1), 501 (± 1), 455 (± 1) and 442 (± 1) ppm, respectively. One trip (f: 9 May 2020) was conducted after the COVID-19 restrictions, with an average of 501 (± 5) ppm.

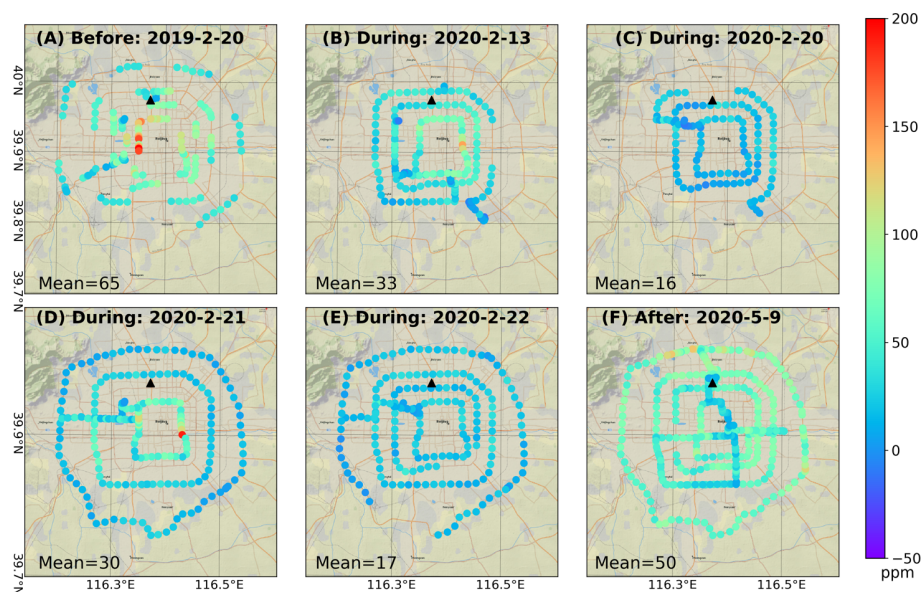


Figure 5. Maps of the CO₂ enhancement for all six trips calculated by subtracting the IAP tower measurements from the on-road CO₂ measurements matched temporally. All subplots have the same color scale, ranging from -50 to 200 ppm. One trip (a: 20 February 2019) was conducted before the COVID-19 restrictions, with an average of 65 (± 0.2) ppm. Four trips (b–e: 13, 20, 21 and 22 February 2020) were conducted during the COVID-19 restrictions, with averages of 33 (± 1.1), 16 (± 1.1), 30 (± 1.1) and 17 (± 1.1) ppm, respectively. One trip (f: 9 May 2020) was conducted after the COVID-19 restrictions, with an average of 50 (± 5.1) ppm.

during the BC and AC trips. This difference is consistent with the spatial distribution mentioned before and is most likely due to background CO₂ fluctuations.

In Fig. 6c, all DC enhancements were generally lower than the BC and AC enhancements, and the statistics for different time periods are listed in Table 3. However, we also found small enhancements for BC and AC, similar to those for DC. For example, the AC enhancement at 12:00–16:00 LST was almost the same as the DC enhancement at that time. By examining the trip routes (Fig. 6d), we found that during that period, the on-road observation vehicle was not driving on the main ring roads. As another example, the BC enhancement at 18:00 LST indicates that the enhancement decreased in a stepwise manner, also because the vehicle drove on other roads (Fig. 6d).

The mean enhancement for the whole BC trip was 65 (± 0.2) ppm, and the average for the evening rush hours (100 ± 0.2 ppm) was 2 times that for the working hours (54 ± 0.2 ppm). This result implies that the increase in vehicle volume during the evening rush hours leads to large traffic emissions and an increase in the on-road CO₂ concentration. For DC, all trips covered the working hours, with a low enhancement of approximately 20 ppm. There was no obvious difference between weekdays and weekends during working hours. The reason may be that the government encouraged people to work remotely at home. Therefore, even on weekdays, according to traffic conditions, the commute volume was low (Fig. S2). Among these four trips, two (on 13 and 20 February 2020) covered the evening rush hours with high averaged enhancements of 55 (± 1.1) and 50 (± 1.1) ppm. Therefore, the total average enhancements for these two trips were higher than those for the other two trips, which covered only working hours. For AC, on 9 May 2020, although it was a Saturday, many residents chose to go out of town for the weekends. The morning rush hours still existed, with a high enhancement of 80 (± 5.1) ppm, and then during the working hours, the enhancement decreased to 46 (± 5.1) ppm.

The comparison of trips showed that the average CO₂ enhancement for the four DC trips was 41 (± 1.3) and 26 (± 6.2) ppm lower than that for the BC and AC trips, respectively. The average AC enhancement was 15 (± 5.3) ppm lower than the average BC enhancement. This difference may be caused by two factors. (1) The first relates to “weekly effects”; a previous study also suggested that, compared to that during weekdays, the average daily traffic CO₂ emissions during weekends in the north part of the fifth ring road (LinCui Road – Anli Road, 3 km) decreased by 5 % in 2014 (Zheng et al., 2020). (2) Until 9 May 2020, although there were approximately 30 d without increases in COVID-19 cases in Beijing, the city was still under level-2 response control; social life was recovering but had not yet completely recovered.

6.4 Analysis of CO₂ enhancement for independent time periods and roads

According to the previous analysis, we found that enhancement exhibited a strong correlation with time (rush or working hours) and road type. Therefore, we statistically analyzed the CO₂ enhancement according to the road type and time period, as shown in Fig. 7. In Fig. 7a, on 13 and 20 February 2020, the CO₂ concentrations on the other, second and fourth, ring roads and all roads were at the same levels as those during the BC and AC trips. However, in Fig. 7b, the four DC enhancements were generally lower than those during AC and BC for all road types. Although on the second ring road, the DC enhancements on 13 and 21 February 2020 were almost the same as the BC and AC enhancements, the DC trips were during rush hours, whereas the AC and BC trips were during working hours. Some very high deviations also occurred (rush hours on the other roads: second and fifth ring roads), which indicates the dispersion of the CO₂ enhancement. The reason for this difference is that we classified all roads excluding the ring roads as other roads, which may have included arterial and residential roads, so the different road types may have increased the deviation. For the second and fifth ring roads, high deviation occurred because during rush hour, traffic flow and transportation varied greatly and resulted in drastic changes in the CO₂ enhancement, which also caused much higher deviations. After a statistical significance test, we found that the CO₂ enhancement difference between working times and rush hours for all trips was significant ($p < 0.02$, assuming that $\alpha = 0.05$). The CO₂ enhancement for BC was also significantly different from that for DC ($p < 0.05$); however, the difference between the AC and BC enhancements was not significant. This suggests that the decreased CO₂ enhancement observed during the COVID-19 restrictions was significantly different from those before and after the COVID-19 restrictions. We also calculated specific statistics, which are listed in Table 4.

7 Discussion

7.1 Analysis of the correlation with traffic flow

It was difficult to obtain a quantitative evaluation of the influence of COVID-19 restrictions on CO₂ emissions from traffic because of limited data. In this study, we found that the one-trip enhancement for DC (on 21 February 2020, with weather conditions and a route that were the most similar to those for the BC and AC trips) was 30 (± 1.1) ppm. The enhancement accounted for 46 % of that for BC (65 ± 0.2 ppm), and the enhancement for AC (50 ± 5.1 ppm) accounted for 77 % of that for BC. Here, we adopted four datasets and methods to explain our hypothesis that the decrease in traffic volume led to a reduction in on-road CO₂ emissions and concentration during the COVID-19 restrictions. First, according to the “anal-

Table 3. CO₂ enhancement (mean and instrumental uncertainties) for six trips over different periods (ppm). Times are indicated in LST.

Label	Observation date	Weather condition	Total average (07:00–20:00)	Morning rush hours (07:00–09:00)	Working hours (09:00–17:00)	Evening rush hours (17:00–20:00)
BC	2019-2-20 (Wed)	Clear	65 (± 0.2)	–	54 (± 0.2)	100 (± 0.2)
DC						
	2020-2-13 (Thu)	Stable/heavy pollution	33 (± 1.1)	–	26 (± 1.1)	55 (± 1.1)
	2020-2-20 (Thu)	Stable/light pollution	16 (± 1.1)	–	16 (± 1.1)	–
	2020-2-21 (Fri)	Windy day	30 (± 1.1)	–	16 (± 1.1)	50 (± 1.1)
	2020-2-22 (Sat)	Windy day	17 (± 1.1)	–	17 (± 1.1)	–
AC	2020-5-9 (Sat)	Windy day	50 (± 5.1)	80 (± 5.1)	46 (± 5.1)	–
Total BC–DC			41 (± 1.3)	–	35 (± 1.3)	48 (± 1.3)
Total AC–DC			26 (± 6.2)	–	27 (± 6.2)	–

Table 4. Statistical analysis (mean value and 1 standard deviation) of the CO₂ enhancement for six trips according to the time and road type.

Label	Date	Time	Other roads	Second ring road	Third ring road	Fourth ring road	Fifth ring road	All roads	Significance test (<i>p</i>)	
									Working hours compared to rush hours	DC/AC compared to BC
BC										
	2019-2-20 (Wed)	Working hours	31/24	81/26	77/11	56/18	37/8	54/26	0.015	–
		Rush hours	58/37	125/34	–	–	–	100/48		–
		Both	42/33	109/38	77/11	56/18	37/8	65/38	–	–
DC										
	2020-2-13 (Thu)	Working hours	8/16	29/15	38/13	29/11	–	26/18	0.018	–
		Rush hours	10/14	74/20	37/14	–	–	55/31		–
		Both	9/16	63/28	38/13	29/11	–	33/26	–	0.041
	2020-2-20 (Thu)	Working hours	9/13	15/8	14/10	24/8	–	16/11	–	–
		Rush hours	–	–	–	–	–	–	–	
		Both	9/13	15/8	14/10	24/8	–	16/11	–	0.001
	2020-2-21 (Fri)	Working hours	12/13	–	–	25 ± 7	13 ± 7	16 ± 10	0.002	–
		Rush hours	32/17	67/29	–	35/15	–	50/28		–
		Both	20/18	67/29	–	30/13	13/7	30/26	–	0.026
	2020-2-22 (Sat)	Working hours	16/11	22/7	21/8	15/13	–	17/12	–	–
		Rush hours	–	–	–	–	–	–	–	
		Both	16/11	22/7	21/8	15/13	–	17 ± 12	–	0.001
AC										
	2020-5-9 (Sat)	Working hours	30/22	65/18	60/14	57/17	73/18	46/26	0.008	–
		Rush hours	89/28	–	–	–	75/24	81/26		–
		Both	36/29	65/18	60/14	57/17	73/20	50/28	–	0.41

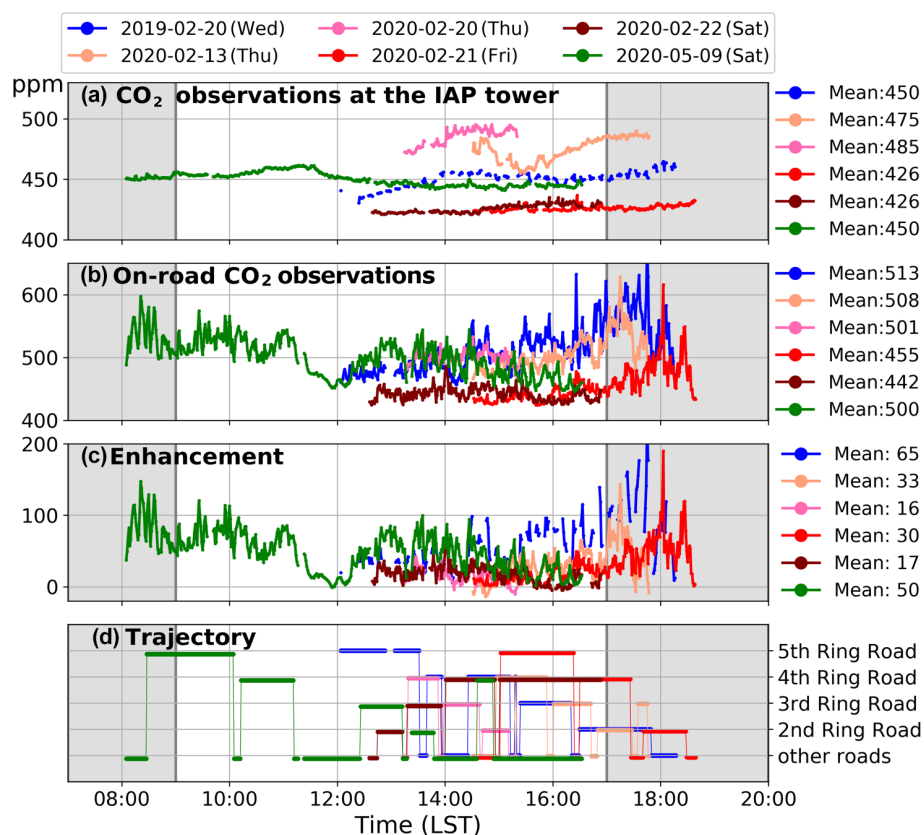


Figure 6. The six trips were plotted on a single day. The two gray regions refer to the morning and evening rush hours. The six colorful lines represent the six trips on different days. Four of the six trips covered at least one (morning and/or evening) rush hour. Panel (a) shows the CO₂ concentration at the IAP tower during the trips. Panel (b) shows the on-road CO₂ concentration. Panel (c) shows the CO₂ enhancements. Panel (d) shows the six trip trajectories.

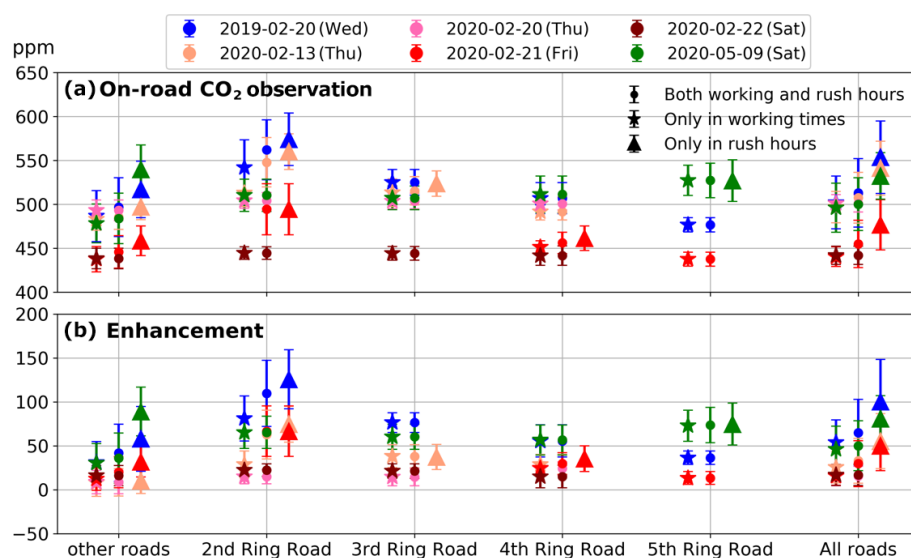


Figure 7. Statistical analysis (mean and 1 standard deviation) of all on-road trips according to the road types and times. Panel (a) shows the on-road CO₂ concentration. Panel (b) shows the CO₂ enhancement.

ysis of road traffic operation in Beijing during COVID-19 in 2020” published by the Beijing Transport Institute, during the first 8 weeks (from 1 February to 31 March, the DC period in this study), the Beijing ground transportation index (calculated based on the ratio of congested road length to the whole road length) decreased by 53 % compared to that on normal days, whereas, from 1 April to 31 May, the index recovered to 92 % (Zhang, 2020). The index implied that traffic flow for DC was dramatically decreased compared to that for BC, and the index for AC almost recovered but not completely. This index variation is consistent with our observations. Second, two remote sensing images from similar dates were adopted (Fig. 8). According to statistics and estimations based on coverage area, we found that the BC traffic flows on the main roads of the fourth and third ring roads were 227 and 226 veh km⁻¹ (vehicles per kilometer), respectively. However, the DC traffic flow decreased to 35 and 34 veh km⁻¹, reflecting a reduction of approximately 85 %. With the assuming that emission factors were the same, the CO₂ emissions on roads for DC may have sharply decreased by approximately 85 % compared to those for BC. This difference is higher than the passenger transportation decrease estimated by Han et al. (2020) (56 % in the first quarter of 2020) because remote sensing images are snapshots and cover only part of the urban area. Moreover, Hans’ results are the average of the first 3 months and the entire Beijing administrative region. Third, we also used traffic congestion condition data, although with low temporal and spatial resolution, to indicate the on-road traffic flow and emissions (Fig. 9). Fourth, the vehicle speed maps of the six trips were plotted (Fig. 10). Overall, these maps reflect the spatial patterns of road traffic conditions during the surveys and could also reflect the specifics on a single road. However, these maps are sensitive to subjective speed variations caused by drivers, such as when facing traffic lights.

7.2 Uncertainty analysis

In this research, uncertainty mainly existed in the following terms:

1. Uncertainty existed from the observation instruments. In this study, four instruments were adopted for measuring CO₂ concentrations: three for on-road observations (a Picarro G2401, with an accuracy of approximately 0.1 ppm; a LI-COR LI-7810, ~ 1 ppm; and a low-cost sensor, no more than 5 ppm) and one for the IAP tower observation (Picarro G2301, ~ 0.1 ppm). During analysis, both the proposed enhancement method and the CO₂ concentration or enhancements of different trips were compared using linear analysis (addition or subtraction). Therefore, the enhancement uncertainties from the observation instruments were ~ 0.2 ppm for BC, ~ 1.1 ppm for DC, less than 5.1 ppm for AC, ~ 1.3 ppm for comparing BC and DC, and less than 6.2 ppm for comparing DC and AC. Note that the stan-

dard deviations shown in Table 4 mainly presented CO₂ concentration fluctuations within specific periods and on certain roads and uncertainty from instruments (relatively small).

2. The IAP tower CO₂ concentration was used as the background from Beijing. In this study, the IAP tower data were adopted as the urban background CO₂ concentration in Beijing. Its measurement footprint was influenced by two factors: wind speed/direction and air intake height. For wind speed/direction, in Beijing, the main wind directions were northwest (winter) and southeast (summer) (Cheng et al., 2018). Generally, high-level data have a large footprint and good representativeness. For example, Cheng et al. (2018) showed that CO₂ data recorded at 280 m height have an average fetch of ~ 17 km, which covers a major part of the city; data collected at 80 m height have an average fetch of ~ 8 km; data collected at 8 m height may have an average fetch of only ~ 230 m; and the fetch at the surface (2 m) may be smaller. Therefore, there are two uncertainties. The first is the height variation during the observation trips. Due to the data availability and for comparison consistency, we chose the lower- and surface-level data. According to Cheng et al. (2018), the CO₂ concentration at the 80 m height is ~ 15 ppm higher than that at the 8 m height. Therefore, if this difference between the lower level and surface level was added, the BC enhancement would increase (~ 15 ppm), which means that the DC enhancement would be even lower (~ 56 ppm) than the BC enhancement. The other is the difference between the surface-level data and 280 m height data in different seasons. According to Cheng et al. (2018), the monthly averaged CO₂ showed a relatively stable difference among the different heights: the CO₂ at the lower level was approximately 40 ppm higher than that at 280 m in February and approximately 30 ppm higher in May. The AC enhancement should increase 10 ppm additionally, which means that the DC enhancement would be even lower (~ 36 ppm) than the AC enhancement. Considering these uncertainties, the results support our hypothesis.
3. Influences of vegetation sinks and natural changes were also prevalent. To understand the CO₂ variability impacted by natural sinks (especially for vegetation), we used the dynamic vegetation and terrestrial carbon cycle model VEGAS (Zeng et al., 2014) to simulate the terrestrial biosphere–atmosphere flux (F_{ta}) in Beijing during 2000–2020 (Fig. S3). The model was run at a 2.5 × 2.5° resolution from 1901 to June 2020, forced by observed climate variables, including monthly precipitation and hourly temperature. Although precipitation and temperature in 2020 were higher than the climatology (average of the last 20 years), the difference between the F_{ta}

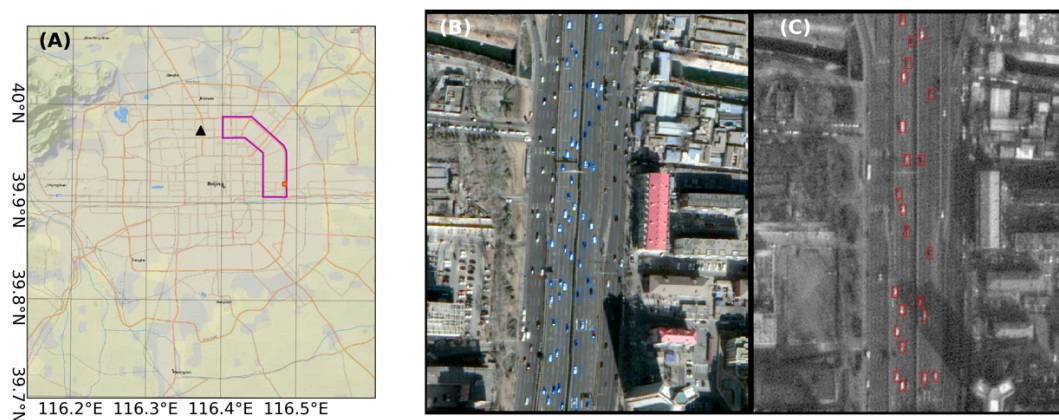


Figure 8. Traffic volume comparison with using remote sensing images. (a) Coverage region of remote sensing images (purple polygon) and example region shown on the right (red square); (b) remote sensing images from Google Earth on 21 February 2019 at 11:42:00 LST, with a spatial resolution of 0.37 m for multispectral band images; 61 vehicles on the main road were interpreted (labeled by blue polygons); (c) remote sensing image from the Beijing-2 satellite on 19 February 2020 at 10:20:08 LST, with a spatial resolution of 0.8 m for the panchromatic band images and 24 vehicles labeled with red polygons.

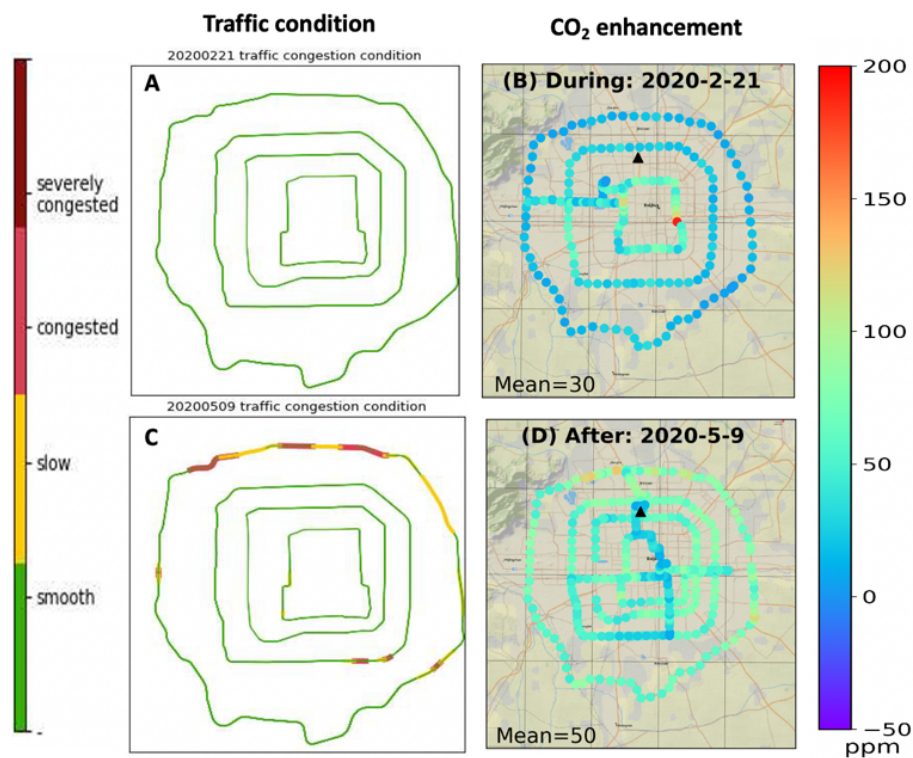


Figure 9. Comparison of traffic conditions with the CO₂ enhancement. (a) Traffic conditions on 21 February 2020; (b) CO₂ enhancement on 21 February 2020; (c) traffic conditions on 9 May 2020; (d) CO₂ enhancement on 9 May 2020.

in 2020 and the average was within 1 standard deviation. This suggests that the Fta in 2020 was not obviously unusual compared to that over the last 20 years. We also analyzed the CO₂ concentration at the Shangdianzi station in the Beijing rural region, which is one of the three WMO/GAW regional stations in China, to determine the CO₂ background variation (Fang et al.,

2016). The results (Fig. S4) showed that the background CO₂ concentration variation mainly induced by natural factors from February to May was only approximately 5 ppm. However, these two factors (vegetation flux and natural changes) both indicate areas far larger than Beijing urban areas. Because the location of the IAP tower and the tracks of the on-road observations are both in

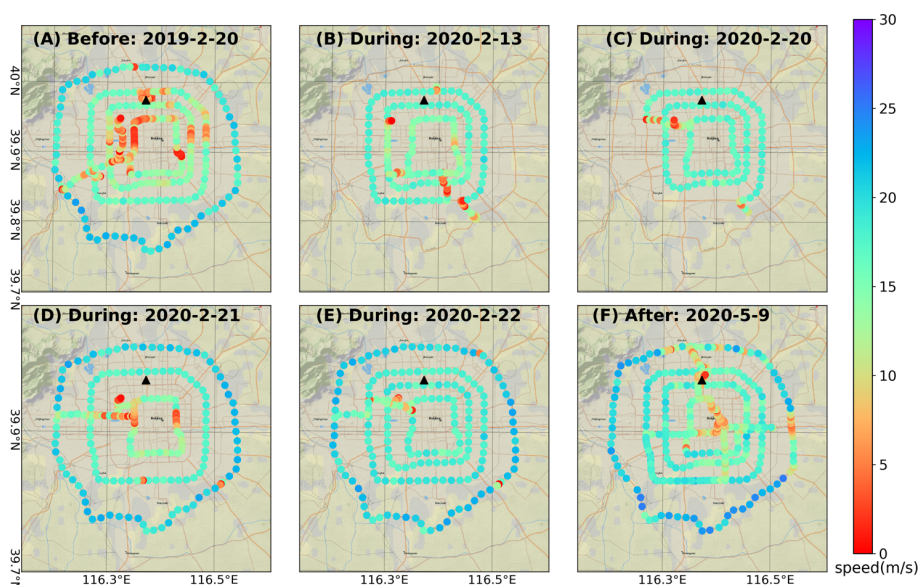


Figure 10. Speed maps of six trips, ranging from 0 to 30 m s⁻¹. One trip (a: 20 February 2019) was conducted before the COVID-19 restrictions. Four trips (b–e: 13, 20, 21 and 22 February 2020) were conducted during the COVID-19 restrictions; one trip (f: 9 May 2020) was conducted after the COVID-19 restrictions.

urban Beijing and we used the enhancement method, these factors were reduced.

4. When data were collected, especially when switching between lower and upper levels, a large amount of data was lost. However, because the data gaps were evenly distributed and the IAP tower CO₂ concentrations were relatively stable, we assumed that it would not affect the final statistical results.
5. In this study, our on-road observations did not have a fixed route or beginning/ending time, which means that the observations on different dates represented different roads. Therefore, we analyzed a wide time range of observations (rush hours, working hours or whole days), which may have also caused uncertainty.

8 Conclusion

The CO₂ emission reduction caused by COVID-19 restrictions is an opportunity to test our ability to collect CO₂ observations in urban areas. In this study, we chose on-road CO₂ concentrations as the target, because ground transportation is the main source of CO₂ in urban areas and was remarkably influenced by policy restrictions due to the COVID-19 pandemic. We conducted six on-road observations in Beijing, including one trip before COVID-19 restrictions, in February 2019; four trips during COVID-19 restrictions, in February 2020; and one trip in May 2020, after COVID-19 restrictions had been eased. The results showed that on-road CO₂ concentrations were strongly affected by traffic emissions

and weather. However, the enhancement metric, which was the difference in the on-road CO₂ concentration and the city “background”, reduced the impact of background CO₂ fluctuations. The results showed that for DC, the total average CO₂ enhancements of the four trips were 41 (±1.3) ppm and 26 (±6.2) ppm lower than those for BC and AC, respectively. Detailed analysis showed that this reduction commonly existed on all road types during the same time period (rush hours/working hours). For the DC trips, there was no significant difference during work hours between weekdays and weekends. The enhancements during rush hours were much higher than those during working hours, and compared with the enhancement reduction during rush hours for BC, that for DC was more obvious. Our findings, which show a clear decrease for DC compared with BC and AC, are consistent with the COVID-19 restrictions, which may be direct evidence of reductions in CO₂ concentrations and carbon emissions. On-road CO₂ observations are an effective way to understand and analyze the urban carbon CO₂ concentration distribution and variation and should be regularly and more frequently conducted in future work. The development and successful application of the miniaturized and low-cost CO₂ monitoring instruments used in this study (Khan et al., 2012; Shusterman et al., 2016; Martin et al., 2017; Müller et al., 2020; Bao et al., 2020) will greatly aid in the collection of on-road observations and even high-density network observations and play a key role in future urban carbon observations.

Code availability. The scripts used in this study are open and can be made available to interested users upon contacting the corresponding author.

Data availability. The data in this study are open and can be made available to interested users upon contacting the corresponding author.

Supplement. The supplement related to this article is available online at: <https://doi.org/10.5194/acp-21-4599-2021-supplement>.

Author contributions. PH, BY and NZ conceived and designed the study. DL summarized the results and wrote the draft of the paper. WS and PH designed and conducted the on-road observations. PW provided the IAP tower observation data. KZ, ZL, HM and QC helped to collect, process and analyze data.

Competing interests. The authors declare that they have no conflict of interest.

Acknowledgements. Special thanks are given to Zhe Hu, Zhimin Zhang and Xiaoli Zhou for collecting the data and conducting the observations.

Financial support. This research has been supported by the Ministry of Science and Technology of the People's Republic of China (grant no. 2017YFB0504000).

Review statement. This paper was edited by Ralf Sussmann and reviewed by two anonymous referees.

References

- Bao, Z., Han, P., Zeng, N., Liu, D., Cai, Q., Wang, Y., Tang, G., Zheng, K., and Yao, B.: Observation and modeling of vertical carbon dioxide distribution in a heavily polluted suburban environment, *Atmos. Ocean. Sci. Lett.*, 13, 371–379, <https://doi.org/10.1080/16742834.2020.1746627>, 2020.
- Bush, S. E., Hopkins, F. M., Randerson, J. T., Lai, C.-T., and Ehleringer, J. R.: Design and application of a mobile ground-based observatory for continuous measurements of atmospheric trace gas and criteria pollutant species, *Atmos. Meas. Tech.*, 8, 3481–3492, <https://doi.org/10.5194/amt-8-3481-2015>, 2015.
- Cheng, X. L., Liu, X. M., Liu, Y. J., and Hu, F.: Characteristics of CO₂ Concentration and Flux in the Beijing Urban Area, *J. Geophys. Res.-Atmos.*, 123, 1785–1801, <https://doi.org/10.1002/2017jd027409>, 2018.
- Fang, S. X., Tans, P. P., Dong, F., Zhou, H., and Luan, T.: Characteristics of atmospheric CO₂ and CH₄ at the Shangdianzi regional background station in China, *Atmos. Environ.*, 131, 1–8, 2016.
- Friedlingstein, P., Jones, M. W., O'Sullivan, M., Andrew, R. M., Hauck, J., Peters, G. P., Peters, W., Pongratz, J., Sitch, S., Le Quéré, C., Bakker, D. C. E., Canadell, J. G., Ciais, P., Jackson, R. B., Anthoni, P., Barbero, L., Bastos, A., Bastrikov, V., Becker, M., Bopp, L., Buitenhuis, E., Chandra, N., Chevallier, F., Chini, L. P., Currie, K. I., Feely, R. A., Gehlen, M., Gilfillan, D., Gkritzalis, T., Goll, D. S., Gruber, N., Gutekunst, S., Harris, I., Haverd, V., Houghton, R. A., Hurtt, G., Ilyina, T., Jain, A. K., Joetzjer, E., Kaplan, J. O., Kato, E., Klein Goldewijk, K., Korsbakken, J. I., Landschützer, P., Lauvset, S. K., Lefèvre, N., Lenton, A., Lienert, S., Lombardozzi, D., Marland, G., McGuire, P. C., Melton, J. R., Metzl, N., Munro, D. R., Nabel, J. E. M. S., Nakaoka, S.-I., Neill, C., Omar, A. M., Ono, T., Peregón, A., Pierrot, D., Poulter, B., Rehder, G., Resplandy, L., Robertson, E., Rödenbeck, C., Séférian, R., Schwinger, J., Smith, N., Tans, P. P., Tian, H., Tilbrook, B., Tubiello, F. N., van der Werf, G. R., Wiltshire, A. J., and Zaehle, S.: Global Carbon Budget 2019, *Earth Syst. Sci. Data*, 11, 1783–1838, <https://doi.org/10.5194/essd-11-1783-2019>, 2019.
- George, K., Ziska, L. H., Bunce, J. A., and Quebedeaux, B.: Elevated atmospheric CO₂ concentration and temperature across an urban-rural transect, *Atmos. Environ.*, 41, 7654–7665, <https://doi.org/10.1016/j.atmosenv.2007.08.018>, 2007.
- Grimmond, C. S. B., King, T. S., Cropley, F. D., Nowak, D. J., and Souch, C.: Local-scale fluxes of carbon dioxide in urban environments: methodological challenges and results from Chicago, *Environ. Pollut.*, 116, S243–S254, [https://doi.org/10.1016/s0269-7491\(01\)00256-1](https://doi.org/10.1016/s0269-7491(01)00256-1), 2002.
- Gross, B., Zheng, Z., Liu, S., Chen, X., Sela, A., Li, J., Li, D., and Havlin, S.: Spatio-temporal propagation of COVID-19 pandemics, *arXiv [preprint]*, <https://arxiv.org/abs/2003.08382> (last access: May 2020), arXiv:2003.08382, 2020.
- Han, P., Cai, Q., Oda, T., Zeng, N., Shan, Y., Lin, X., and Liu, D.: Assessing the recent impact of COVID-19 on carbon emissions from China using domestic economic data, *Sci. Total Environ.*, 750, 141688, <https://doi.org/10.1016/j.scitotenv.2020.141688>, 2020.
- Idso, C. D., Idso, S. B., and Balling, R. C.: The urban CO₂ dome of Phoenix, Arizona, *Phys. Geogr.*, 19, 95–108, <https://doi.org/10.1080/02723646.1998.10642642>, 1998.
- Idso, C. D., Idso, S. B., and Balling, R. C.: An intensive two-week study of an urban CO₂ dome in Phoenix, Arizona, USA, *Atmos. Environ.*, 35, 995–1000, [https://doi.org/10.1016/s1352-2310\(00\)00412-x](https://doi.org/10.1016/s1352-2310(00)00412-x), 2001.
- Idso, S. B., Idso, C. D., and Balling, R. C.: Seasonal and diurnal variations of near-surface atmospheric CO₂ concentration within a residential sector of the urban CO₂ dome of Phoenix, AZ, USA, *Atmos. Environ.*, 36, 1655–1660, [https://doi.org/10.1016/s1352-2310\(02\)00159-0](https://doi.org/10.1016/s1352-2310(02)00159-0), 2002.
- Khan, A., Schaefer, D., Tao, L., Miller, D. J., Sun, K., Zondlo, M. A., Harrison, W. A., Roscoe, B., and Lary, D. J.: Low Power Greenhouse Gas Sensors for Unmanned Aerial Vehicles, *Remote Sens.*, 4, 1355–1368, <https://doi.org/10.3390/rs4051355>, 2012.
- Kutsch, W., Vermeulen, A., Karstens, U.: Finding a hair in the swimming pool: the signal of changed fossil emissions in the atmosphere, available at: <https://www.icos-cp.eu/event/917>, last access: December 2020.
- Le Quere, C., Jackson, R. B., Jones, M. W., Smith, A. J. P., Abernethy, S., Andrew, R. M., De-Gol, A. J., Willis, D. R., Shan, Y.,

- Canadell, J. G., Friedlingstein, P., Creutzig, F., and Peters, G. P.: Temporary reduction in daily global CO₂ emissions during the COVID-19 forced confinement, *Nat. Clim. Change*, 10, 647–653, <https://doi.org/10.1038/s41558-020-0797-x>, 2020.
- LI-COR LI-7810 Brochure: <https://www.licor.com/documents/yldtj3q6jyxx3xnc8680ytx6i0afc9uu> (last access: 20 June 2020), 2019.
- Liu, Z., Ciais, P., Deng, Z., Lei, R., Davis, S. J., Feng, S., Zheng, B., Cui, D., Dou, X., Zhu, B., Guo, R., Ke, P., Sun, T., Lu, C., He, P., Wang, Y., Yue, X., Wang, Y., Lei, Y., Zhou, H., Cai, Z., Wu, Y., Guo, R., Han, T., Xue, J., Boucher, O., Boucher, E., Chevallier, F., Tanaka, K., Wei, Y., Zhong, H., Kang, C., Zhang, N., Chen, B., Xi, F., Liu, M., Bréon, F., Lu, Y., Zhang, Q., Guan, D., Gong, P., Kammen, D. M., He, K., and Schellnhuber, H. J.: Near-real-time monitoring of global CO₂ emissions reveals the effects of the COVID-19 pandemic, *Nat Commun.*, 14, 11, 5172, <https://doi.org/10.1038/s41467-020-18922-7>, 2020.
- Martin, C. R., Zeng, N., Karion, A., Dickerson, R. R., Ren, X., Turpie, B. N., and Weber, K. J.: Evaluation and environmental correction of ambient CO₂ measurements from a low-cost NDIR sensor, *Atmos. Meas. Tech.*, 10, 2383–2395, <https://doi.org/10.5194/amt-10-2383-2017>, 2017.
- Mitchell, L. E., Lin, J. C., Bowling, D. R., Pataki, D. E., Strong, C., Schauer, A. J., Bares, R., Bush, S. E., Stephens, B. B., Mendoza, D., Mallia, D., Holland, L., Gurney, K. R., and Ehleringer, J. R.: Long-term urban carbon dioxide observations reveal spatial and temporal dynamics related to urban characteristics and growth, *P. Natl. Acad. Sci. USA*, 115, 2912–2917, <https://doi.org/10.1073/pnas.1702393115>, 2018.
- Müller, M., Graf, P., Meyer, J., Pentina, A., Brunner, D., Perez-Cruz, F., Hüglin, C., and Emmenegger, L.: Integration and calibration of non-dispersive infrared (NDIR) CO₂ low-cost sensors and their operation in a sensor network covering Switzerland, *Atmos. Meas. Tech.*, 13, 3815–3834, <https://doi.org/10.5194/amt-13-3815-2020>, 2020.
- Ott, L., Peters, G., and Meyer, A.: Special virtual panel: Covid-19 and its impact on global carbon emissions, https://carbon.nasa.gov/policy_speaker_28052020.html (last access: December 2020).
- Perez, I. A., Luisa Sanchez, M., Angeles Garcia, M., and de Torre, B.: CO₂ transport by urban plumes in the upper Spanish plateau, *Sci. Total Environ.*, 407, 4934–4938, [10.1016/j.scitotenv.2009.05.037](https://doi.org/10.1016/j.scitotenv.2009.05.037), 2009.
- Picarro G2401 Analyzer Datasheet: https://www.picarro.com/support/library/documents/g2401_analyzer_datasheet?language=en# (last access: 20 July 2020), 2017.
- Picarro G2301 Analyzer Datasheet: https://www.picarro.com/support/library/documents/g2301_analyzer_datasheet?language=en# (last access: 20 June 2020), 2019.
- Rosenzweig, C., Solecki, W., Hammer, S. A., and Mehrotra, S.: Cities lead the way in climate-change action, *Nature*, 467, 909–911, <https://doi.org/10.1038/467909a>, 2010.
- SenseAir: K30 products sheets: <https://rmtplusstoragesenseair.blob.core.windows.net/docs/publicerat/PSP110.pdf> (last access: 20 July 2020), 2019.
- Shusterman, A. A., Teige, V. E., Turner, A. J., Newman, C., Kim, J., and Cohen, R. C.: The BErkeley Atmospheric CO₂ Observation Network: initial evaluation, *Atmos. Chem. Phys.*, 16, 13449–13463, <https://doi.org/10.5194/acp-16-13449-2016>, 2016.
- Su, T., Li, Z., and Kahn, R.: Relationships between the planetary boundary layer height and surface pollutants derived from lidar observations over China: regional pattern and influencing factors, *Atmos. Chem. Phys.*, 18, 15921–15935, <https://doi.org/10.5194/acp-18-15921-2018>, 2018.
- Sun, W., Deng, L., Wu, G., Wu, L., Han, P., Miao, Y., and Yao, B.: Atmospheric Monitoring of Methane in Beijing Using a Mobile Observatory, *Atmosphere-Basel*, 10, <https://doi.org/10.3390/atmos10090554>, 2019.
- Sussmann, R. and Rettinger, M.: Can We Measure a COVID-19-Related Slowdown in Atmospheric CO₂ Growth? Sensitivity of Total Carbon Column Observations, *Remote Sens.*, 12, 2387, <https://doi.org/10.3390/rs12152387>, 2020.
- Woodwell, G. M., Houghton, R. A., and Tempel, N. R.: Atmospheric CO₂ at Brookhaven, Long-Island, New-York – Patterns of Variation up to 125 Meters, *J. Geophys. Res.*, 78, 932–940, <https://doi.org/10.1029/JC078i006p00932>, 1973.
- Zeng, N., Zhao, F., Collatz, G. J., Kalnay, E., Salawitch, R. J., West, T. O., and Guanter, L.: Agricultural Green Revolution as a driver of increasing atmospheric CO₂ seasonal amplitude, *Nature*, 515, 394–397, <https://doi.org/10.1038/nature13893>, 2014.
- Zhang, Y.: Analysis of road traffic operation in Beijing during COVID-19 in 2020, available at: <https://mp.weixin.qq.com/s/AtSXWtK4LvzI7UPuJTHvIQ>, last access: August 2020 (in Chinese).
- Zhang, Z., Wong, M., and Lee, K.: Estimation of potential source regions of PM_{2.5} in Beijing using backward trajectories, *Atmos. Pollut. Res.*, 6, 173–177, <https://doi.org/10.5094/apr.2015.020>, 2015.
- Zheng, J., Dong, S., Hu, Y., and Li, Y.: Comparative analysis of the CO₂ emissions of expressway and arterial road traffic: A case in Beijing, *Plos One*, 15, e0231536, <https://doi.org/10.1371/journal.pone.0231536>, 2020.